Progress In Electromagnetics Research, Vol. 153, 57–68, 2015

Broadband Calculations of Band Diagrams in Periodic Structures Using the Broadband Green's Function with Low Wavenumber Extraction (BBGFL)

Leung Tsang*

Abstract—We apply the method of the Broadband Green's Functions with Low wavenumber extraction (BBGFL) to calculate band diagrams in periodic structures. We consider 2D impenetrable objects placed in a 2D periodic lattice. The low wavenumber extraction is applied to the 2D periodic Green's function for the lattice which is used to formulate the surface integral equation. The low wavenumber extraction accelerates the convergence of the Floquet modes expansion. Using the BBGFL to the surface integral equation and the Method of Moments gives a linear eigenvalue equation that gives the broadband (multi-band) solutions simultaneously for a given point in the first Brillouin zone. The method only requires the calculation of the periodic Green's function at a single low wavenumber. Numerical results are illustrated for the 2D hexagonal lattice to show the computational efficiency and accuracy of the method. Because of the acceleration of convergence, an eigenvalue problem with dimensions 49 plane wave Floquet modes are sufficient to give the multi-band solutions that are in excellent agreement with results of the Korringa Kohn Rostoker (KKR) method. The multiband solutions for the band problem and the complementary band problem are also discussed.

1. INTRODUCTION

The calculation of band diagrams is a fundamental subject and has numerous applications for periodic structures in electron waves, microwaves, photonic crystals, metamaterials, volumetric EBG, acoustics etc. A common method is the plane wave method [1–6]. The Korringa Kohn Rostoker method (KKR) [7, 8] and the multiple scattering method MST [9, 10] were also applied. These two methods used wave expansions to treat circular/spherical scatterers and have high accuracy. The use of Ewald summation was also used to speed up the calculations of the periodic Green's function [9]. Recently, discrete methods such as the finite difference time domain method (FDTD) [11–13], and the finite element method (FEM) [14–17] were also used. The MoM/BIRME method and the IE/BIRME method were also used in calculations of band diagrams in planar and closed metallic electromagnetic bandgap structures [18, 19]. The advantages of the plane wave method are simple implementation and that the eigenvalue problem is linear with the broadband solutions, i.e., all the bands, calculated simultaneously. The disadvantage of the method is the poor convergence of the plane wave Floquet mode expansion. In the plane wave method, a spectral expansion of the potential function or permittivity is taken. This spectral expansion has accuracy issues for large contrasts between the objects and the background medium. The KKR method and the MST have high accuracy but is CPU intensive [5]. The method also requires a nonlinear search for the band solution with one band at a time.

In this paper, the periodic Green's function of the periodic lattice is used to formulate surface integral equation. The periodic Green's function has slow convergence. If the periodic Green's function

Received 29 August 2015, Accepted 8 October 2015, Scheduled 15 October 2015

* Corresponding author: Leung Tsang (leutsang@umich.edu).
The author is with the Radiation Laboratory, Department of Electrical Engineering and Computer Science, The University of Michigan, Ann Arbor, 48109-2122 MI, USA.

is used for the surface integral equation to calculate the eigenvalues, the equation is nonlinear and an iterative search needs to be performed with one band at a time. Recently, the Broadband Green's Function with Low wavenumber extraction (BBGFL) [20–23] has been applied to wave propagation in waveguide/cavity of arbitrary shape. By using a single low wavenumber extraction, the convergence of the modal expansion of the Green's function is accelerated. Also the singularity of the Green's function has been extracted. The method has been shown to be efficient for broadband simulations of wave propagation in waveguides/cavity. It is noted that the modal expansion of Green's function in a waveguide is similar in form to the Floquet expansion of Green's function in a periodic structure. In this paper we adapt the BBGFL to calculate band diagrams in periodic structures. We use a low wavenumber extraction to accelerate the convergence of the periodic Green's function.The BBGFL is used to formulate the surface integral equations. Next applying the Method of Moments gives a linear eigenvalue equation that gives all the multi-band solutions simultaneously for a point in the first Brillouin zone. We label this as "broadband simulations" as the multi-band solutions are calculated simultaneously rather than searching the band solution one at a time. The multiband solutions of the band problem and the multi-band solutions of the complementary band problem are calculated simultaneously. Numerical results are illustrated to show the computational efficiency and accuracy of the method. In Section 2, we formulate the scattering problem of PEC scatterers in a periodic structure.The BBGFL is then applied to the periodic Green's function. The method is then combined with the Method of Moments. In Section 3, numerical results are illustrated for circular impenetrable objects using size parameters that are representative [9]. The case of hexagonal lattice is illustrated. Because of the acceleration of convergence, an eigenvalue problem with dimensions of 49 Floquet modes are sufficient to give the multi-band solutions that are in good agreement with the results of the KKR method. The multiband solutions of the complementary problem are also discussed.

2. FORMULATION

Consider a 2D periodic lattice (Figure 1) in xy plane with z perpendicular to the plane. We use the following notations. A lattice translation is invariant for

$$\bar{R}_{pq} = p\bar{a}_1 + q\bar{a}_2 \tag{1}$$

where $\bar{a}_1$ and $\bar{a}_2$ are the primitive translation vectors, and p, q are integers, $-\infty < p, q < \infty$.

We label the cell by index (p, q).

The reciprocal lattice vectors are

$$\bar{K}_{pq} = p\bar{b}_1 + q\bar{b}_2 \tag{2}$$

where $-\infty < p, q < \infty$.

$$\bar{b}_1 = 2\pi \frac{\bar{a}_2 \times \hat{z}}{\Omega_0} \tag{3a}$$

$$\bar{b}_2 = 2\pi \frac{\hat{z} \times \bar{a}_1}{\Omega_0} \tag{3b}$$

and $\Omega_0 = |\bar{a}_1 \times \bar{a}_2|$ is the size of the unit cell.

Let $\bar{k}_i$ be a wave vector in the first Brillouin zone, where

$$\bar{k}_i = \beta_1\bar{b}_1 + \beta_2\bar{b}_2 \tag{4}$$

where $0 \le \beta_1, \beta_2 \le \frac{1}{2}$.

Then the Floquet (Bloch) mode vector is

$$\bar{k}_{ipq} = \bar{k}_i + \bar{K}_{pq} \tag{5}$$

Then in the spectral domain, the periodic Green's function for a given $\bar{k}_i$ and $k = \omega\sqrt{\mu\varepsilon}$ is

$$g_p\left(k, \bar{k}_i; x, y, x', y'\right) = \frac{1}{\Omega_0} \sum_{p,q} \frac{1}{\left|\bar{k}_{ipq}\right|^2 - k^2} \exp\left(i\bar{k}_{ipq} \cdot \left(\bar{\rho} - \bar{\rho}'\right)\right) \tag{6}$$

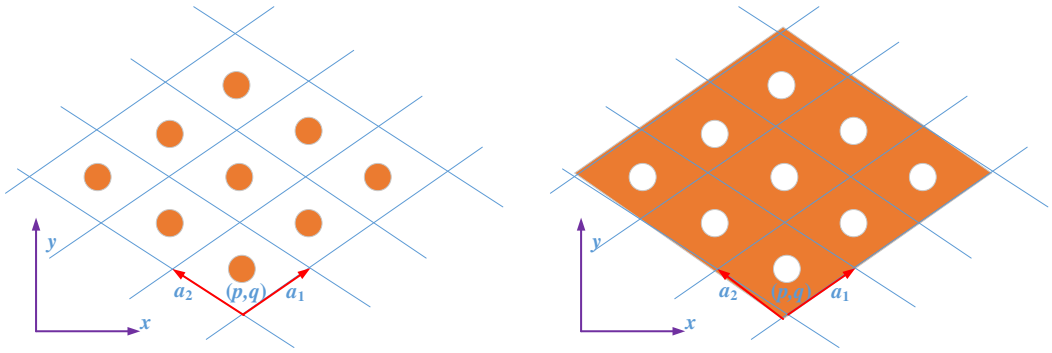

(a) real problem (b) complementary problem

Figure 1. 2D periodic lattice: (a) Band problem consists of PEC for scatterers and permittivity ε for background; (b) complementary band problem consists of permittivity ε for scatterers and PEC for background.

The factor $\exp(i\bar{k}_{ipq}\cdot(\bar{\rho}-\bar{\rho}'))$ is the Floquet (Bloch) mode. We next use a combined Greek index $\alpha=(p,q)$. Then

$$g_p\left(k,\bar{k}_i;x,y,x',y'\right)=\frac{1}{\Omega_0}\sum_{\alpha}\frac{1}{\left|\bar{k}_{i\alpha}\right|^2-k^2}\exp\left(i\bar{k}_{i\alpha}\cdot\left(\bar{\rho}-\bar{\rho}'\right)\right) \tag{7}$$

Note that the above expansion is similar to the waveguide mode expansion [23]. In the problem considered in this paper, the band problem consists of the scatterer being perfect electric conductor and the background has permittivity ε (Figure 1(a)). The complementary band problem has the roles reversed so that the scatterer has permittivity ε and the background is PEC (Figure 1(b)). We consider waves that obey the Dirichlet boundary conditions on the surface of the cylinder.

The cylinder in cell (0, 0) is labelled as the 0-th cylinder and the cylindrical surface is labelled as S_{00} with $\hat{n}$ the outward normal to S_{00}. The region inside the (0, 0) cylinder is labelled as A_{00}.

For the band problem, the integral equation is

$$\int_{S_{00}}dl'g_P\left(k,\bar{k}_i;\bar{\rho}-\bar{\rho}'\right)\left[\hat{n}'\cdot\nabla'\psi\left(x',y'\right)\right]=0,\quad for\ (x,y)\ in\ A_{00} \tag{8}$$

where ψ is the wave function which is the z component of the electric field for the TM waves of the case of electromagnetics. For the complementary band problem, the integral equation is

$$\int_{S_{00}}dl'g_P\left(k,\bar{k}_i;\bar{\rho}-\bar{\rho}'\right)\left[\hat{n}'\cdot\nabla'\psi\left(x',y'\right)\right]=\psi(x,y),\quad for\ (x,y)\ in\ A_{00} \tag{9}$$

Equation (8) is the starting point of the KKR method (Appendix A). Let t be the coordinate on the boundary so that $(x,y)=(x(y),y(t))$ be a point on the boundary. Then the surface integral equation is obtained by letting (x,y) approach S_{00} from A_{00}. This is performed for both (8) and (9). Then

$$\int_{S_{00}}dl'g_P\left(k,\bar{k}_i;x,y,x',y'\right)J_s\left(t'\right)=0 \tag{10}$$

where $(x(t),y(t))$ and $(x',y')=(x(t'),y(t'))$ are both on the surface of the circular cylinder. In (10), the surface current is $J_s\left(t'\right)=\hat{n}'\cdot\nabla'\psi\left(x',y'\right)$. Note that we get the same surface integral equation for the band problem and the complementary problem. Thus solving (10) will give solutions for the multi-bands of the band problem and the complementary multi-bands.

We solve surface integral equation to find the multiple values of k for the given $\bar{k}_i$. The multivalues correspond to the different bands for the same $\bar{k}_i$. The difficulties of the approach are

(i) the expansion $\Sigma_{p,q}$ has slow convergence,

(ii) the search for k is a nonlinear search that requires calculations of $g_P\left(k,\bar{k}_i;x,y,x',y'\right)$ at many k's,

(iii) the search for k is one solution at a time, in order to obtain multiple k in multiband solutions.

In the following we describe the BBGFL that are to circumvent the above three problems.

We choose a low wavenumber k_L. Then we apply BBGFL, in a manner similar to waveguide/cavity problem [20–23]. The periodic Green's function is expressed as the sum of the Green's function at that single low wavenumber k_L and the Floquet mode expansion with that low wavenumber counterpart subtracted. Then

$$g_P\left(k,\bar{k}_i;\bar{\rho},\bar{\rho}'\right)=g_P\left(k_L,\bar{k}_i;\bar{\rho},\bar{\rho}'\right)+\frac{k^2-k_L^2}{\Omega_0}\sum_\alpha\frac{1}{\left(\left|\bar{k}_{i\alpha}\right|^2-k^2\right)\left(\left|\bar{k}_{i\alpha}\right|^2-k_L^2\right)}\exp\left(i\bar{k}_{i\alpha}\cdot\left(\bar{\rho}-\bar{\rho}'\right)\right) \quad (11)$$

The above is known as BBGFL (Broadband Green's Functions with Low wavenumber extraction) as it has simple frequency dependence in $(k^2-k_L^2)/(|\bar{k}_{i\alpha}|^2-k^2)$. It has two parts, the low wavenumber extraction $g_P(k_L,\bar{k}_i;\bar{\rho},\bar{\rho}')$ and the Floquet modal expansion. The low wavenumber part has no wavenumber dependence. The mode expansion has convergence of $|\bar{k}_{i\alpha}|^4$ and converges even at the point $\bar{\rho}=\bar{\rho}'$.

The procedure requires the calculation of $g_P(k,\bar{k}_i;\bar{\rho},\bar{\rho}')$ only at a single $k=k_L$. We then further decompose the calculated $g_P(k_L,\bar{k}_i;\bar{\rho},\bar{\rho}')$ into free space Green's function and response

$$g_P\left(k_L,\bar{k}_i;\bar{\rho},\bar{\rho}'\right)=g_0\left(k_L;\bar{\rho},\bar{\rho}'\right)+g_R\left(k_L,\bar{k}_i;\bar{\rho},\bar{\rho}'\right) \quad (12)$$

where

$$g_0\left(k_L;\bar{\rho},\bar{\rho}'\right)=\frac{i}{4}H_0^{(1)}\left(k_L\left|\bar{\rho}-\bar{\rho}'\right|\right) \quad (13)$$

and the response $g_R(k_L,\bar{k}_i;\bar{\rho},\bar{\rho}')$ can be calculated since we already calculated $g_P(k_L,\bar{k}_i;\bar{\rho},\bar{\rho}')$.

Next we substitute $g_P(k,\bar{k}_i;\bar{\rho},\bar{\rho}')$ into the surface integral equation. The impedance matrix element has two parts, one part $Z_{mn}^{(L)}$ due to the low wavenumber extraction and the other $Z_{mn}^{(F)}$ due to the Floquet mode expansion. The singularity at $\bar{\rho}=\bar{\rho}'$ has been extracted and resides in $g_0(k_L;\bar{\rho},\bar{\rho}')$. We use MoM with pulse basis functions and point matching. The scatterer boundary is divided into N patches. The impedance matrix elements are

$$Z_{mn}=Z_{mn}^{(L)}+Z_{mn}^{(F)} \quad (14)$$

where $1\le m,\ n\le N$, $\bar{\rho}_n$ is the center of the n-th patch, $n=1,2,\ldots,N$. The point matching is at $\bar{\rho}_m$, $m=1,2,\ldots,N$.

We discretize into arc length Δt.

The low wavenumber part is

$$Z_{mn}^{(L)}=\left[g_0\left(k_L;\bar{\rho}_m,\bar{\rho}_n\right)+g_R\left(k_L,\bar{k}_i;\bar{\rho}_m,\bar{\rho}_n\right)\right]\Delta t,\quad \text{for } n\ne m \quad (15a)$$

$$Z_{mn}^{(L)}=\frac{i\Delta t}{4}\left[1+i\frac{2}{\pi}\left[\ln\left(\frac{\gamma k_L\Delta t}{4}\right)-1\right]\right]+g_R\left(k_L,\bar{k}_i;\bar{\rho}_m,\bar{\rho}_m\right)\Delta t,\quad \text{for } n=m \quad (15b)$$

where $\gamma=1.78107$ is the Euler's constant. The modal expansion part is

$$Z_{mn}^{(F)}=\frac{k^2-k_L^2}{\Omega_0}\sum_\alpha\frac{1}{\left(\left|\bar{k}_{i\alpha}\right|^2-k^2\right)\left(\left|\bar{k}_{i\alpha}\right|^2-k_L^2\right)}\exp\left(i\bar{k}_{i\alpha}\cdot\left(\bar{\rho}_m-\bar{\rho}_n\right)\right)\Delta t \quad (16)$$

The matrix equation for the surface integral equation becomes

$$\sum_n Z_{mn}^{(L)}J_n+\sum_n Z_{mn}^{(F)}J_n=0 \quad (17)$$

where $J(t)=J_n$ on the nth patch. The matrix equation above can be converted to a linear eigenvalue equation that all the eigenvalues can be solved simultaneously due to the broadband nature of the Green's function. Let N be the number of points in MoM discretization.

There are two discretizations $\alpha=(p,q)$ is the Floquet mode index, while m and n are the indices for MoM point matching and patch discretization.

For the p,q index, we truncate by $-N_{\max}<p,\ q<N_{\max}$. Thus $M=(2N_{\max}+1)^2$. Since the mode expansion is fast convergent with the low wavenumber extraction, M is much less than that without the extraction.

To reexpress $Z_{mn}^{(F)}$, we let

$$R_{m\alpha} = \frac{1}{\sqrt{\Omega}_0} \frac{\exp\left(i\bar{k}_{i\alpha} \cdot \bar{\rho}_m\right)}{\left(\left|\bar{k}_{i\alpha}\right|^2 - k_L^2\right)} \tag{18}$$

The Greek index is $\alpha = 1, 2, \ldots, M$ while the Roman index is $m = 1, 2, \ldots, N$. Then

$$\sum_{n=1}^{N} L_{mn} q_n + \left(k^2 - k_L^2\right) \sum_{n=1}^{N} \sum_{\alpha=1}^{M} \frac{\left|\bar{k}_{i\alpha}\right|^2 - k_L^2}{\left|\bar{k}_{i\alpha}\right|^2 - k^2} R_{m\alpha} R_{n\alpha}^* q_n = 0 \tag{19}$$

where

$$q_n = \Delta t J_n \tag{20}$$

$$Z_{mn}^{(L)} = L_{mn} \Delta t \tag{21}$$

Next, let

$$W_{\alpha\beta} = \frac{1}{\dfrac{1}{k^2 - k_L^2} - \dfrac{1}{\left|\bar{k}_{i\alpha}\right|^2 - k_L^2}} \delta_{\alpha\beta} \tag{22}$$

$$D_{\alpha\beta} = \frac{1}{\left|\bar{k}_{i\alpha}\right|^2 - k_L^2} \delta_{\alpha\beta} \tag{23}$$

where $\delta_{\alpha\beta}$ is the Kronecker delta function. Then

$$\left(k^2 - k_L^2\right) \frac{\left|\bar{k}_{i\alpha}\right|^2 - k_L^2}{\left|\bar{k}_{i\alpha}\right|^2 - k^2} = \frac{1}{\dfrac{1}{k^2 - k_L^2} - \dfrac{1}{\left|\bar{k}_{i\alpha}\right|^2 - k_L^2}} = \sum_{\beta=1}^{M} W_{\alpha\beta} \tag{24}$$

We then get

$$\sum_{n=1}^{N} L_{mn} q_n + \sum_{n=1}^{N} \sum_{\beta=1}^{M} \sum_{\alpha=1}^{M} R_{m\alpha} W_{\alpha\beta} R_{n\beta}^* q_n = 0 \tag{25}$$

In matrix notations

$$\bar{\bar{L}} \bar{q} + \bar{\bar{R}} \bar{\bar{W}} \bar{\bar{R}}^{\dagger} \bar{q} = 0 \tag{26}$$

where $\bar{\bar{R}}^{\dagger}$ is the Hermitian adjoint of $\bar{\bar{R}}$. The matrix $\bar{\bar{R}}$ is of dimension $N \times M$. The matrices $\bar{\bar{W}}$ and $\bar{\bar{D}}$ are $M \times M$ diagonal matrices.

Next let

$$\bar{b} = \bar{\bar{W}} \bar{\bar{R}}^{\dagger} \bar{q} \tag{27}$$

The $\bar{b}$ column vector is of dimension $M \times 1$.

Then

$$\bar{\bar{L}} \bar{q} + \bar{\bar{R}} \bar{b} = 0 \tag{28}$$

Note that

$$\frac{1}{k^2 - k_L^2} \bar{\bar{W}} - \bar{\bar{D}} \bar{\bar{W}} = \bar{\bar{I}} \tag{29}$$

$$\bar{\bar{W}} = \left(\frac{1}{k^2 - k_L^2} \bar{\bar{I}} - \bar{\bar{D}}\right)^{-1} \tag{30}$$

Substitute in (27)

$$\frac{1}{k^2 - k_L^2} \bar{b} - \bar{\bar{D}} \bar{b} = \bar{\bar{R}}^{\dagger} \bar{q} \tag{31}$$

From (28)

$$\bar{q} = -\bar{\bar{L}}^{-1} \bar{\bar{R}} \bar{b} \tag{32}$$

Substitute (32) into (31), the eigen-problem becomes

$$\bar{\bar{A}}\bar{b} = \frac{1}{k^2 - k_L^2}\bar{b} \tag{33}$$

where

$$\bar{\bar{A}} = \bar{\bar{D}} - \bar{\bar{R}}^{\dagger}\bar{\bar{L}}^{-1}\bar{\bar{R}} \tag{34}$$

is of dimension $M \times M$. Thus the eigenvalue problem of Equation (33) is of dimension M which is the number of Floquet modes.

Note that $\bar{\bar{A}}$ is independent of wavenumber (frequency) k.

Solving the eigenvalue problem is a linear eigenvalue problem with all the eigenvalues $1/(k^2 - k_L^2)$ (bands) calculated simultaneously. The eigenvectors $\bar{b}$ are also calculated. The surface current $J_s(t')$ is then calculated by using Equations (32) and (20). Then the wave function $\psi(x, y)$ can be calculated by

$$\psi(x, y) = \int_{S_{00}} dl' g_P\left(k, \bar{k}_i; x, y, x', y'\right) J_s\left(t'\right) \tag{35}$$

where (x, y) can be anywhere inside or outside the cylinder. Equation (35) can be used to determine whether the eigenvalue is a real band (mode) solution or that of the complementary band solution.

3. NUMERICAL RESULTS

We consider the example of a 2D hexagonal lattice defined by the lattice vectors $\bar{a}_1 = \frac{a}{2}(\sqrt{3}\hat{x} + \hat{y})$, and $\bar{a}_2 = \frac{a}{2}(-\sqrt{3}\hat{x} + \hat{y})$. Consider an array of impenetrable circular cylinders of radius b in the lattice. Let $a = 1$, and the permittivity be $\varepsilon = 8.9\varepsilon_0$, where ε_0 is the free space permittivity. We consider two cases, $b = 0.2$, and $b = 0.4$.

Let $\bar{k}_i$ be a wave vector in the first Brillouin zone as defined in Equation (4).

For each $\bar{k}_i$, the multi-band solutions give the multiple k's. For each k, we calculate the normalized frequency f_N by

$$f_N(k) = \frac{k}{2\pi}\sqrt{\frac{\varepsilon_0}{\varepsilon}} \tag{36}$$

In the results, we used k_L so that $f_N(k_L) = 0.001$. We have also used $f_N(k_L) = 0.2$ and 0.5, and both give very similar results. Thus the choice of the low wavenumber k_L is robust.

Case 1: $b = 0.2$, $\varepsilon = 8.9\varepsilon_0$, $a = 1$

We first consider the case when the wave vector is

$$\begin{aligned} \beta_1 &= 0.1 \\ \beta_2 &= 0.05 \end{aligned}$$

In Table 1, we list the f_N for 10 eigenvalues. Three different $N_{\max}$ are chosen to truncate the Floquet modes: ($N_{\max} = 3$, $M = 49$), ($N_{\max} = 5$, $M = 121$), ($N_{\max} = 20$, $M = 1681$). The KKR solutions are also listed. The results with ($N_{\max} = 3$, $M = 49$) agree with KKR to 2 significant figures. The results with ($N_{\max} = 5$, $M = 121$) agree with KKR to 3 significant figures. This shows the BBGFL method is efficient and accurate. The surface currents of several eigenvalues are illustrated in Figure 2. In the table the mode $f_N = 0.642$ is that of the complementary band because the surface integral equation gives the solution of the band problem as well as the complementary band problem. On the other hand, the KKR method (Appendix A) only gives the solutions for the real band problem. For the case of PEC, the complementary band problem corresponds to the TM waveguide solution of $J_n(kb) = 0$, where J_n is Bessel function of nth order. This can also be established by using Equation (35) to calculate the wave outside the cylinder and the wave turns out to be zero outside the cylinder.

We next calculate the band diagram for the first 9 bands, (not including the complementary band). The band diagram of the lattice structure are computed using the BBGFL approach and plotted in Figure 3 using ($M \approx 600$). The KKR results are also shown at selected points. The agreement of the results of BBGFL and that of KKR are excellent.

Case 2: $b = 0.4$, $\varepsilon = 8.9\varepsilon_0$, $a = 1$

Table 1. Comparison of band eigenvalues f_N computed from BBGFL using different number of Floquet modes $(N_{\max}, M)$ after low wavenumber extraction. The results are compared against the KKR results. Results are computed for $\bar{k}_i = 0.1\bar{b}_1 + 0.05\bar{b}_2$. The 7-th mode 0.642 is shown to be a complementary band solution by testing the scattering field outside the PEC cylinder. The geometry parameters are as specified for case 1.

order	BBGFL $N_{\max} = 3$ $M = 49$	BBGFL $N_{\max} = 5$ $M = 121$	BBGFL $N_{\max} = 20$ $M = 1681$	KKR	Root of
1	0.215	0.215	0.215	0.215	
2	0.368	0.368	0.368	0.368	
3	0.413	0.413	0.413	0.413	
4	0.438	0.438	0.438	0.438	
5	0.523	0.523	0.523	0.523	
6	0.528	0.527	0.527	0.526	
7	0.645	0.643	0.642	None	$J_0(kb), 0.639$
8	0.670	0.670	0.669	0.669	
9	0.685	0.684	0.684	0.684	
10	0.705	0.704	0.704	0.704	

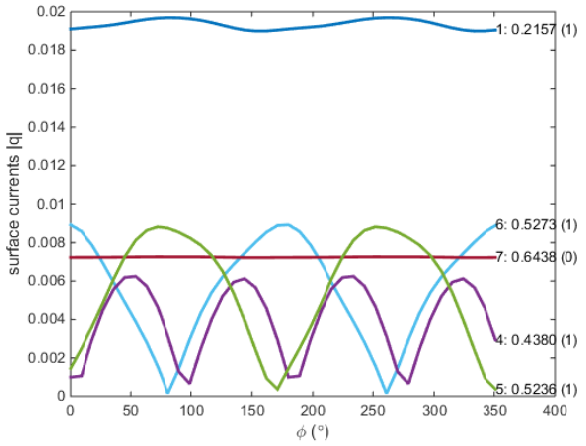

Figure 2. Surface currents of 5 band solutions: (e.g., 4 : 0.4380 means the normalized frequency of the fourth mode ordered in ascending order is 0.4380). The 7-th mode of $f_N = 0.6438$ indicated by "(0)" is that of the complementary band. The modes indicated by "(1)" are real band solution. Results are computed for $\bar{k}_i = 0.1\bar{b}_1 + 0.05\bar{b}_2$. The geometry parameters are as specified for case 1. Results are computed with $M \approx 600$.

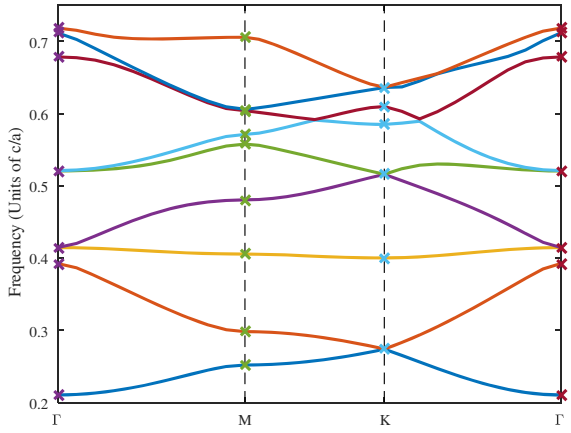

Figure 3. Band diagram of the hexagonal structure with background dielectric constant of 8.9 and PEC cylinders with radius $b = 0.2a$. The lowest 9 bands (not including the complementary band) are plotted in the first irreducible Brillouin zone for the TM waves (Dirichlet boundary condition) shown as solid lines. Results are compared with KKR approach at Γ, M, and K points. KKR results are plotted as cross marks.

The area ratio of scatterers to background is $\pi b^2/\Omega_0 = 58\%$. In Table 2, we list f_N for the first 10 eigenvalues with $\bar{k}_i = 0.1\bar{b}_1 + 0.05\bar{b}_2$. The results with three different $N_{\max}$ to truncate the Floquet modes are compared against the KKR solutions. The BBGFL solutions have both multi-band solutions and the complementary multi-band solutions. The results are in good agreement with that of KKR.

The surface currents corresponding to 5 of the first 10 solutions are plotted in Figure 4.

In Figure 5, we draw the band diagram for the crystal structure with periodic PEC cylinders of radius $b = 0.4a$. Only the four physical band out of the first 10 eigenvalues are shown. The KKR results are also computed at the Γ, M, and K points. The results are in good agreement.

Table 2. Comparison of band eigenvalues f_N computed from BBGFL using different number of Floquet modes. The results are compared against the KKR results. Results are computed for $\bar{k}_i = 0.1\bar{b}_1 + 0.05\bar{b}_2$. The geometry parameters are as specified for case 2.

order	BBGFL $N_{\max} = 3$ $M = 49$	BBGFL $N_{\max} = 5$ $M = 121$	BBGFL $N_{\max} = 20$ $M = 1681$	KKR	Root of
1	0.322	0.322	0.322	None	$J_0(kb), 0.321$
2	0.513	0.512	0.512	None	$J_1(kb), 0.511$
3	0.513	0.513	0.512	None	$J_1(kb), 0.511$
4	0.598	0.594	0.593	0.589	
5	0.611	0.608	0.607	0.604	
6	0.689	0.687	0.687	None	$J_2(kb), 0.685$
7	0.690	0.687	0.687	None	$J_2(kb), 0.685$
8	0.742	0.739	0.738	None	$J_0(kb), 0.736$
9	0.828	0.817	0.815	0.809	
10	0.847	0.820	0.817		

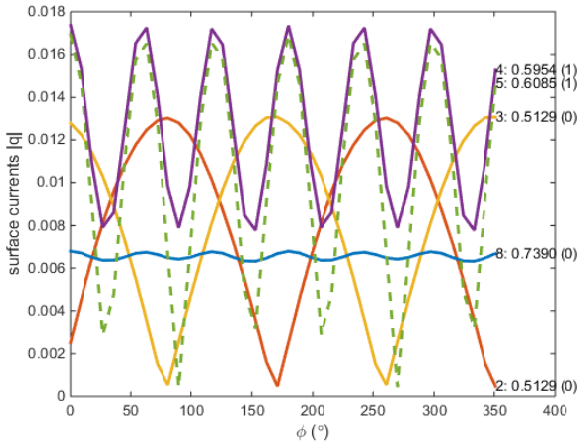

Figure 4. Surface currents of the band solutions: (e.g., 5 : 0.6085 means the normalized frequency of the fifth mode in ascending order is 0.6085). The 4th and 5th eigenvalues are band solutions, as indicated by "(1)" in the plot following the mode frequency. The rest 3 modes as indicated by "(0)" are that of complementary bands. Results are computed for $\bar{k}_i = 0.1\bar{b}_1 + 0.05\bar{b}_2$. The geometry parameters are as specified for case 2. Results are computed with $M \approx 600$.

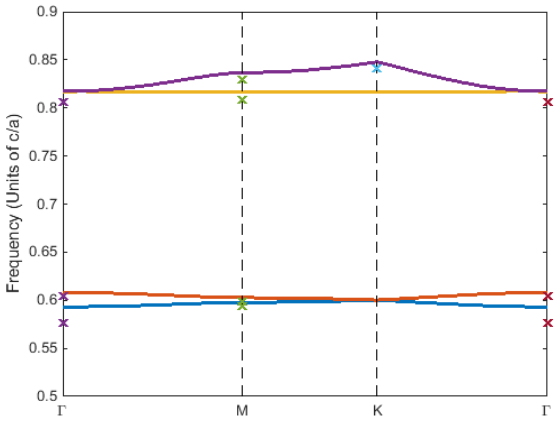

Figure 5. Band diagram of the hexagonal structure with background dielectric constant of 8.9 and PEC cylinders with radius $b = 0.4a$. The lowest 4 bands (not including the complementary multi-bands) are plotted in the first irreducible Brillouin zone for TM waves (Dirichlet boundary condition) shown as solid lines. Results are compared with KKR approach at Γ, M, and K points. KKR results are plotted as cross marks.

Table 3. The CPU time in seconds for computing results in Figures 3 and 5. The time is recorded on an HP ProDesk 600 G1 desktop with Intel® Core™ i7-4790 CPU @ 3.60 GHz and 32 GB RAM. Note the time used to compute the complete band diagram is approximately 30 times the CPU time for one $\bar{k}_i$ since the exact CPU time varies from run to run.

Time in seconds	Compute $g_R(k_L, \bar{k}_i; \bar{\rho}_m, \bar{\rho}_n)$ and $Z_{mn}^{(L)}$, sec	Multi-bands eigen-matrix solution (33) for one $\bar{k}_i$, sec	Total multi-bands solution for one $\bar{k}_i$, sec	the complete band diagram using $30\bar{k}_i$, sec
Figure 3	3.836	0.714	4.550	138.715
Figure 5	3.744	0.728	4.472	142.435

In Table 3, we list the CPU for the results of band diagrams in Figures 3 and 5. Mat lab® was used in computing the band diagram. We compute the solutions for each $\bar{k}_i$ in the Brillouin zone. For each $\bar{k}_i$, we compute the low wavenumber part of $g_R\left(k_L, \bar{k}_i; \bar{\rho}_m, \bar{\rho}_n\right)$ and $Z_{mn}^{(L)}$. Next we compute the multiband solutions for the eigenvalues and eigenvectors of Equation (33). The multiband solutions are computed simultaneously. Adding the two CPU gives the CPU of the multiband solutions for one $\bar{k}_i$. In Figures 3 and 5, we use 30 $\bar{k}_i$ points in the Brillouin zone. The CPU is the product of that of one $\bar{k}_i$ and the number of points of $\bar{k}_i$. The comparison of CPU with KKR is approximate as KKR needs to search iteratively for each band solution, requiring many values of k search for one $\bar{k}_i$. A crude estimate is that the BBGFL method is about 100 times faster than KKR. The procedure of calculation of $g_R(k_L, \bar{k}_i, \bar{\rho}, \bar{\rho}')$ is described in Appendix B.

4. CONCLUSIONS

In this paper we have adapted the BBGFL method, previously applied to waveguide/cavity problems [20–23], to calculate band solutions of periodic structures in 2D problem with 2D periodicity. We considered the case of Dirichlet boundary conditions. The method is shown to be computationally efficient and accurate. The multiband solutions are calculated simultaneously rather than an iterative search on each root. The method is illustrated for the 2D hexagonal lattice. In the low wavenumber extraction, the choice of the low wavenumber k_L is robust. The use of low wavenumber extraction makes the BBGFL method applicable to general lattices. We are extending the method to dielectric scatterers in a dielectric background for the 2D problem. We are also extending the method to 3D problem with 3D periodicity. Since surface integral equation is solved using MoM, the BBGFL method can be applied to scatterers of arbitrary shapes.

APPENDIX A. KKR METHOD

In this appendix, we summarize the governing equations for the KKR method for the case when the PEC cylinder is circular with radius b. The procedure follows that of reference [9]. For the band problem, we use Equation (8). The solution outside the cylinder is expressed as

$$\psi\left(\bar{\rho}\right) = \sum_m c_m J_m\left(k\rho\right) \exp\left(im\phi\right) \tag{A1}$$

On the surface of the cylinder, the surface unknown is

$$\hat{n} \cdot \nabla\psi\left(x, y\right) = \sum_m c_m k J'_m\left(kb\right) \exp\left(im\phi\right) \tag{A2}$$

The periodic Green's function is expressed as

$$g_P\left(k, \bar{k}_i, \bar{\rho} - \bar{\rho}'\right) = -\frac{1}{4} N_0\left(k\left|\bar{\rho} - \bar{\rho}'\right|\right) + \sum_m D_m J_m\left(k\left|\bar{\rho} - \bar{\rho}'\right|\right) \exp\left(im\phi_{\bar{\rho}\bar{\rho}'}\right) \tag{A3}$$

where N_m is Neumann function of mth order.

Since $\rho' = b$ and $\rho < \rho'$, using addition theorem of cylindrical waves [24] gives

$$g_P\left(k, \bar{k}_i, \bar{\rho} - \bar{\rho}'\right) = -\frac{1}{4}\sum_n J_n\left(k\rho\right)\exp\left(in\phi\right)N_n\left(kb\right)\exp\left(-in\phi'\right) + \sum_{m'} D_{m'}\sum_n J_n\left(k\rho\right)\exp\left(in\phi\right)J_{n-m'}\left(kb\right)\exp\left(-i\left(n-m'\right)\phi'\right) \tag{A4}$$

Substituting into (8), integrate over ϕ' and since the set $J_n\left(k\rho\right)\exp\left(in\phi\right)$ is complete, we have the matrix equation,

$$\sum_m Q_{nm}c_m = 0 \tag{A5}$$

where

$$Q_{nm} = D_{n-m}\left[-J_m\left(kb\right)kJ'_m\left(kb\right)\right] + \frac{\delta_{nm}}{4}N_m\left(kb\right)kJ'_m\left(kb\right) \tag{A6}$$

Let

$$\bar{c} = \bar{\bar{P}}\bar{d} \tag{A7}$$

where

$$P_{mm'} = \frac{1}{-J_m\left(kb\right)kJ'_m\left(kb\right)}\delta_{mm'} \tag{A8}$$

Then

$$\bar{\bar{\Lambda}}\bar{d} = 0 \tag{A9}$$

where

$$\Lambda_{nm} = D_{n-m} - \frac{\delta_{nm}}{4}\frac{N_m\left(kb\right)}{J_m\left(kb\right)} \tag{A10}$$

The band solution is given by

$$\det\bar{\bar{\Lambda}}\left(k\right) = 0 \tag{A11}$$

The solution requires an iterative search, with band solution of one k at a time. Unlike the surface integral equation, the KKR solution only has that of the band problem of Equation (8), and not Equation (9) of the complementary band problem.

APPENDIX B. CALCULATION OF $g_R(k_L, \bar{k}_i; \bar{\rho}, \bar{\rho}')$

The low wavenumber part of the impedance matrix is $Z^{(L)}_{mn}$. In computing $Z^{(L)}_{mn}$, we note from (15a) and (15b) that we need to compute the response part, $g_R(k_L, \bar{k}_i; \bar{\rho}, \bar{\rho}')$, of the periodic Green's function once at the low wavenumber k_L. Note that $g_R(k_L, \bar{k}_i; \bar{\rho}, \bar{\rho}')$ is a smooth function and only depends on $\bar{\rho} - \bar{\rho}'$. We use the following efficient procedure.

For $\bar{\rho} \neq 0$,

$$g_P\left(k, \bar{k}_i; \bar{\rho}\right) = \frac{1}{\Omega_0}\sum_{\alpha=1}^{M_L}\frac{\exp\left(i\bar{k}_{i\alpha}\cdot\bar{\rho}\right)}{\left|k_{i\alpha}\right|^2 - k_L^2} \tag{B1}$$

Then using Equations (A3) and (B1) and integrating $g_P\left(k, \bar{k}_i; \bar{\rho}\right)$ over a circle of radius $|\bar{\rho}| = R_1$, we obtain the expression of the coefficients $D_n\left(k, \bar{k}_i\right)$

$$D_n\left(k, \bar{k}_i\right) = \frac{1}{J_n\left(kR_1\right)}\left[\frac{i^n}{\Omega_0}\sum_{\alpha=1}^{M_L}J_n\left(\left|k_{i\alpha}\right|R_1\right)\frac{\exp\left(-in\phi_{k_{i\alpha}}\right)}{\left|k_{i\alpha}\right|^2 - k_L^2} + \frac{1}{4}N_0\left(kR_1\right)\delta_{n0}\right] \tag{B2}$$

where $\phi_{k_{i\alpha}}$ is the polar angle of the vector $\bar{k}_{i\alpha}$ and R_1 is an arbitrary radius. After $D_n(k, \bar{k}_i)$ coefficients are obtained, the $g_R(k, \bar{k}_i; \bar{\rho})$ is calculated by

$$g_R\left(k, \bar{k}_i; \bar{\rho}\right) = \sum_n C_n\left(k, \bar{k}_i\right)\frac{J_n\left(k\rho\right)}{J_n\left(kR_2\right)}\exp\left(in\phi\right) \tag{B3}$$

where

$$C_n\left(k,\bar{k}_i\right)=\left(D_n\left(k,\bar{k}_i\right)-\frac{1}{4}\delta_{n0}\right)J_n\left(kR_2\right) \tag{B4}$$

In Equations (B3) and (B4), R_2 is chosen to have better normalization of the coefficients $C_n(k,\bar{k}_i)$.

In the BBGFL procedure, Equations (B2), (B3) and (B4) are calculated only once at the wavenumber k_L. We choose $M_L=(401)^2$.

Note that M_L is different from M. The quantity M is the truncation of BBGFL which is small. On the other hand M_L is used to evaluate the periodic Green's function at $|\bar{\rho}-\bar{\rho}'|=R_1$ and $k=k_L$. Thus M_L is much larger than M. Since the surface integral equation is solved on the surface of the scatterer so that $0\leq|\bar{\rho}-\bar{\rho}'|\leq 2b$ in the MoM implementation, we choose $R_1=R_2=2b$. For the coefficients, we calculate $C_n(k_L,\bar{k}_i)$ and $D_n(k_L,\bar{k}_i)$ for $|n|\leq 4$.

REFERENCES

1. Ho, K. M., C. T. Chan, and C. M. Soukoulis, "Existence of a photonic gap in periodic dielectric structures," *Physical Review Letters*, Vol. 65, 3152–3155, 1990.
2. Leung, K. M. and Y. F. Liu, "Full vector wave calculation of photonic band structures in face-centered-cubic dielectric media," *Physical Review Letters*, Vol. 65, 2646–2649, 1990.
3. Plihal, M. and A. A. Maradudin, "Photonic band structure of two-dimensional systems: The triangular lattice," *Phys. Rev. B*, Vol. 44, No. 16, 8565–8571, 1991.
4. Mead, R. D., K. D. Brommer, A. M. Rappe, and J. D. Joannopoulos, "Existence of a photonic bandgap in two dimensions," *Applied Physics Letters*, Vol. 61, 495–497, 1992.
5. Kafesaki, M. and C. M. Soukoulis, "Historical perspective and review of fundamental principles in modelling three-dimensional periodic structures with emphasis on volumetric EBGs," *Metamaterials*, N. Engheta and R. W. Ziolkowski (eds)., Chapter 8, John Wiley and Sons, 2006.
6. Joannopoulos, J. D., S. G. Johnson, J. N. Winn, and R. D. Meade, *Photonic Crystals: Molding the Flow of Light*, Princeton University Press, 2011.
7. Korringa, J., "On the calculation of the energy of a Bloch wave in a metal," *Physica*, Vol. 13, No. 6, 392–400, 1947.
8. Kohn, W. and N. Rostoker, "Solution of the Schrödinger equation in periodic lattices with an application to metallic lithium," *Phys Rev.*, Vol. 94, 1111–1120, 1954.
9. Leung, K. M. and Y. Qiu, "Multiple-scattering calculation of the two-dimensional photonic band structure," *Physical Review B*, Vol. 48, No. 11, 7767–7771, 1993.
10. Liu, Z., C. T. Chan, P. Sheng, A. L. Goertzen, and J. H. Page, "Elastic wave scattering by periodic structures of spherical objects: Theory and experiment," *Physical Review B*, Vol. 62, 2446–2457, 2000.
11. Taflove, A. and S. Hagness, *Computational Electrodynamics: The Finite-difference Time-domain Method*, Artech House, Boston, 2000.
12. Fan, S., P. R. Villeneuve, and J. D. Joannopoulos, "Large omnidirectional band gaps in metallodielectric photonic crystals," *Physical Review B*, Vol. 54, 11245–11251, 1996.
13. Ziolkowski, R. W. and M. Tanaka, "FDTD analysis of PBG waveguides, power splitters and switches," *Optical and Quantum Electronics*, Vol. 31, 843–855, 1999.
14. Hiett, B. P., J. M. Generowicz, S. J. Cox, M. Molinari, D. H. Beckett, and K. S. Thomas, "Application of finite element methods to photonic crystal modelling," *IEE Proc-SciMeasurment Technology*, Vol. 149, 293–296, 2002.
15. Jin J.-M. and D. J. Riley, *Finite Element Analysis of Antennas and Arrays*, Hoboken, Wiley, 2009.
16. Jin, J.-M., *The Finite Element Method in Electromagnetics*, John Wiley & Sons, 2014.
17. Luo, M., Q. H. Liu, and Z. Li, "Spectral element method for band structures of two-dimensional anisotropic photonic crystals," *Physical Review E*, Vol. 79, 026705, 2009.

18. Bozzi, M., S. Germani, L. Minelli, L. Perregrini, and P. de Maagt, "Efficient calculation of the dispersion diagram of planar electromagnetic band-gap structures by the MoM/BI-RME method," *IEEE Trans. on Antennas and Propagation*, Vol. 53, No. 1, 29–35, Jan. 2005.
19. Marini, S., A. Coves, V. E.Boria, and B. Gimeno, "Efficient modal analysis of periodic structures loaded with arbitrarily shaped waveguides," *IEEE Trans. on Microwave Theory and Tech.*, Vol. 58, No. 3, 529–536, 2010.
20. Tsang, L. and S. Huang, "Full wave modeling and simulations of the waveguide behavior of printed circuit boards using a broadband Green's function technique," Provisional U.S. Patent No. 62/152.702, Apr. 24, 2015.
21. Huang, S., "Broadband Green's function and applications to fast electromagnetic analysis of high-speed interconnects," Ph.D. Dissertation, Dept. Elect. Eng., Univ. Washington, Seattle, WA, Jun. 2015.
22. Huang, S. and L. Tsang, "Broadband Green's function and applications to fast electromagnetic modeling of high speed interconnects," *IEEE International Symposium on Antennas and Propagation*, Vancouver, BC, Canada, Jul. 2015.
23. Tsang, L. and S. Huang, "Broadband Green's function with low wavenumber extraction for arbitrary shaped waveguide and applications to modeling of vias in finite power/ground plane," *Progress of Electromagnetic Research*, Vol. 152, 105–125, 2015.
24. Tsang, L., J. A. Kong, K. H. Ding and C. O. Ao, *Scattering of Electromagnetic Waves, Vol. 2: Numerical Simulations*, 705 pages, Wiley Interscience, 2001.